Hydrogen Dispersion in a full-scale road tunnel: Experimental results and CFD analysis

C. Melin[1], E. Studer[1], D. Forero[1], G. Bernard-Michel[1], D. Bouix[2], F. Sauzedde[2]

[1] Univ. Paris-Saclay, CEA, Service de Thermohydraulique et de Mécanique des Fluides, F-91191 Gif-sur-Yvette, France
[2] Univ. Grenoble Alpes, CEA, LITEN, F-38000 Grenoble, France

ABSTRACT

Hydrogen Fuel Cell Electric Vehicles (HFC EVs) represent an alternative to replace current internal combustion engine vehicles. The use of these vehicles with storage of compressed gaseous hydrogen (CGH2) in confined spaces, such as tunnels, underground car parks, etc., creates new challenges to ensure the protection of people and property and to keep the risk at an acceptable level. The HYTUNNEL-CS project sponsored by the FCH-JU was launched to develop validated hazard and risk assessment tools for the behavior of hydrogen leaks in tunnels. Among the experiments carried out in support of the validation tools, the CEA has conducted tests on gas dispersion in a full-scale tunnel geometry. In the tests carried out, hydrogen is replaced by helium under a pressure of 70 MPa in a 78 liter tank. The car is simulated by a flat plate called chassis and the discharges are made either downwards under the chassis, or upwards to take into account a rollover of the car during the accident. Different thermally activated pressure relief device (TPRD) diameters are examined as well as different orientations of the discharge. Finally, the mixing transient of helium with air is measured for distances between -50 and +50m from the release. Performing CFD simulations of such an under-expanded jet in an environment as large as a road tunnel demands a compressible flow solver, and so a large computational cost. To optimize this cost, a notional nozzle approach is generally used to replace the under-expanded jet by a subsonic jet that has the same concentration dilution behavior. The physics at the injection point is then not resolved and a model of these boundary conditions has to be implemented. This article first reviews the main experimental results. Then, a model of boundary conditions is proposed to have a subsonic hydrogen jet that matches the dilution characteristics of an under-expanded jet. Furthermore, this model is implemented in the TRUST LES computer code and in the Neptune-CFD RANS computer code in order to simulate some helium dispersion experiments. Finally, results from the CFD simulations are compared to the experimental results and the effect of the exact shape of the tunnel is also assessed by comparing simulations with idealized flat walls and real scanned walls.

1.0 Introduction

Hydrogen Fuel Cell Electric Vehicles (HFC EVs) represent an alternative to replace current internal combustion engine vehicles. The use of these vehicles with storage of compressed gaseous hydrogen (CGH2) or cryogenic liquid hydrogen (LH2) in confined spaces, such as tunnels, underground car parks, etc., creates new challenges to ensure the protection of people and property and to keep the risk at an acceptable level. Several studies have shown that confinement or congestion can lead to severe accidental consequences compared to accidents in an open atmosphere. It is therefore necessary to develop validated hazard and risk assessment tools for the behavior of hydrogen leaks in tunnels

In the past, hydrogen gas releases in a tunnel-like geometry have been carried out by SRI at the Corral Hollow Experiment Site **[1]** in a scaled-down facility. The tube representing the tunnel was 78.5 m long and had a diameter of only 2.4 m. An embankment was located in the lower part to form a horseshoe shaped cross-section of 3.74 m². Sato et al. **[2]** described some hydrogen release experiments corresponding to TPRD release scenarios for vehicles to leaks on transported hydrogen bottles. The releases were carried out through a tube located 15 cm above the road and oriented upwards. The scenarios were scaled using the method described by Hall et al **[3]**. The hydrogen concentrations measured in the experiments showed that the maximum concentration was always above the point of

release whether or not ventilation was activated. The inertial effect of the jet played a major role, which is dominant for an upward discharge. Moving away from the nozzle, the hydrogen concentration decreased rapidly. Ventilation can greatly reduce the hydrogen concentration when the discharges are less inertial. All release scenarios studied led to lean mixtures and maximum concentrations of 9 vol% were mentioned. More recently, Houf at al. **[1]** described experiments carried out in the same facility but for a scenario corresponding to simultaneous opening of three TPRDs under a simplified vehicle represented by a hexahedron. This scenario led to very high hydrogen concentrations. The measured values reached up to 40% hydrogen volume near the ceiling at the discharge location and a concentration close to stoichiometry at 3m downstream of the release. Under the chassis, concentrations close to 100% were measured. Simulations carried out with the FLACS code confirmed these values. Many other numerical simulations were available in the literature i.e. Venetsanos et al. **[4]**, Middha et al. **[5]**, Bie et al. **[6]** and Li et al **[7]**. For scenarios involving cars with a 70 MPa pressure tank without ventilation (worst case), Venetsanos et al. obtained a maximum flammable volume of 519 m^3 (3.7 kg of hydrogen) for a release trough a 6 mm TPRD approximately 20 seconds after the start of the release. Middha et al. calculated a maximum flammable volume of 270 m^3 (1.33 kg) if the 4 mm TPRD releases hydrogen downwards and 280 m^3 (1.14 kg) for an upward release. For Houf et al, the simultaneous opening of three TPRDs led to a maximum flammable volume of between 390 and 450 m^3 depending on the ventilation rate and this maximum was reached between 10 and 20 seconds after the start of the release. Bie et al. did not provide the size of the flammable cloud but only calculated concentrations of around 5 vol% hydrogen at 5 meters from the discharge in the axis of the tunnel after a few seconds. It should be noted that in the latter case, the release was vertical upwards at the rear of the vehicle with a TPRD of 6 mm. Finally, Li et al. presented a release calculation with a TPRD of 2.25 mm upwards and obtained 16 seconds after the start of the release a sensible volume (layered TDD criterion) of approximately 72 m^3 for a mass of 2.9 kg of hydrogen. In all these cases, there is a limited number of experimental data for model validation and especially no full-scale data.

Two experimental campaigns have been carried out, one in 2020 and one in 2021. The former was previously described in **[8]** and this paper describes the 2021 one. Consequently, the experimental is only briefly described. Then, the helium dispersion tests are detailed with their main conclusions about the effect of the size of the TPRD and its orientation. Two tests are then selected for numerical simulations. The numerical models are described as well as the boundary conditions, including the modelling adopted for the under-expanded jet. Finally, comparisons between experiments and calculations are analysed and conclusions follow.

2.0 Experimental results

2.1 Test geometry and test matrix

The tests were performed in the tunnel du Mortier (near Autrans village, Isère, France). This disused road tunnel has a horse-shoe type cross-section with a total length of about 502 m. The slope is 3.6% and the tunnel is divided in two different sections. The one located on the Autrans side is made of a flat concrete ceiling arch. The second one on the Montaud side is made of raw limestone rocks. The injection device was installed in this second section for the 2021 tests whereas for the 2020 tests it was located in the concrete section. The tunnel dimensions vary in the rocky section, an average height is close to 5.9 m, and the diameter is about 8.9 m. Two sidewalks are also present on each side of the road. The chassis, a flat plate (1.9x4.5m) representing the size of a real car was parallel to the road (Figure 1 a) and between 230 to 250 mm above it. The calibrated orifice representing the TPRD of a real compressed gaseous hydrogen storage was located at the rear of the chassis and it was oriented upward (UP), downward (DW) with an angle of 45° to the rear.

The monitoring system can be divided into two parts:

- The one related to the injection tank and the release pipes. Relative pressures and gas temperature were recorded inside the tank (P_0, T_0), at the outlet of the tank (P_1, T_1) and upstream the calibrated orifice (P_2, P_{2bis} and T_2). These were used to check the mass balance and compute the release flowrate.

- The one related to the tunnel (Figure 1 b, c and d). Ten vertical masts were used to support the measuring devices in the upper part of the tunnel. Additional supporting structures were installed around the chassis on the lower part to monitor the downward releases. These sensors were mainly helium concentration measurement (Xe and He catharometers) and thermocouples (Tk). Oxygen concentration sensors (Ox) were also installed to confirm the helium concentration measurements. Ultrasonic wind sensors monitored the convection flow in the tunnel during the tests.

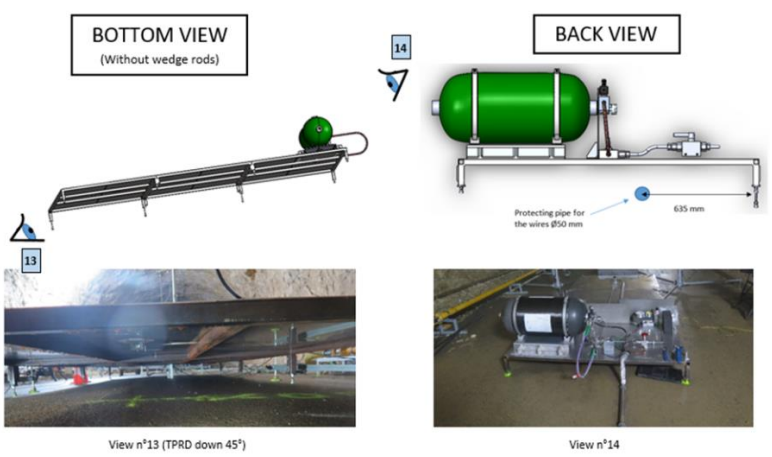

a) Details of the chassis

b) 10 vertical masts

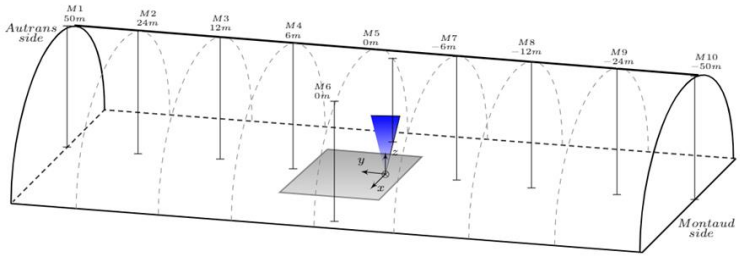

c) Schematic description of the tests

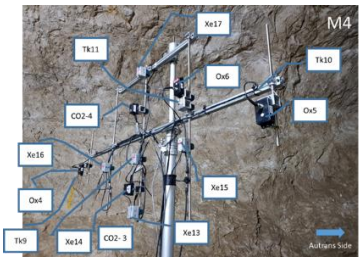

d) Sensors on mast M4

Figure 1: Pictures of the test geometry

Three experiments (tests 02, 05 and 07) were performed with 60 to 70 MPa helium tanks of 78 L volume following a preliminary experimental campaign in 2020 of seven tests with 20 MPa 50 L tanks. The first test (test 01) was therefore intended to reproduce a 2 mm upward release with 20 MPa 50 L tank performed in 2020 but under the rocky vault. Then, the comparison between the results of tests 01 and 02 enables to quantify the effect of the increase in storage pressure and of larger quantities. Comparison between tests 02 and 05 allows quantifying the effect of release orientation (UP and DW). Finally, the effect of release diameter for a downward release of 45° can be assessed by comparing tests 05 (2 mm) and 07 (1 mm).

2.2 Experimental results

For test 01, maximum concentrations around 1 vol% (Figure 2 a) were measured close to the ceiling similar to 2020 test. However, the flow of the natural ventilation (~0.3 m/s before injection) of the tunnel was directed towards Autrans (Figure 1 c) and consequently only the sensors located in this direction measure helium.

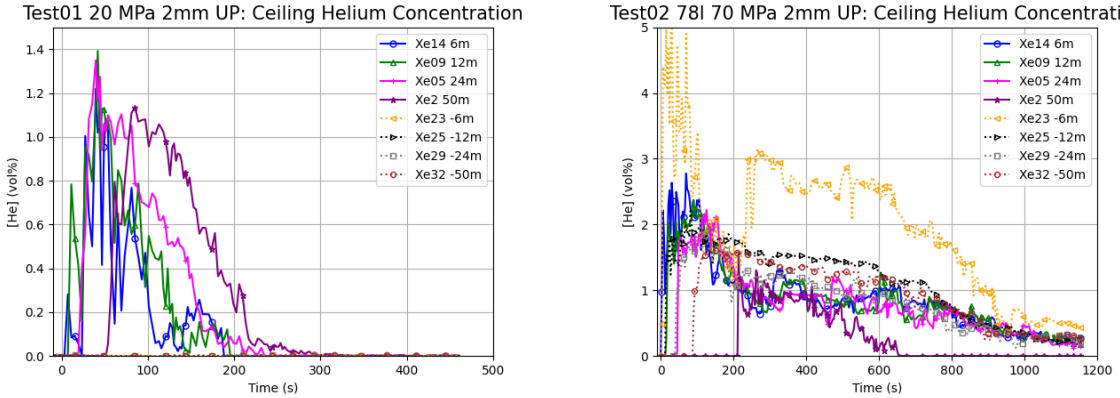

a) Test 01: 2mm TPRD UP 20 MPa, 50 l Type II

b) Test 02: 2mm TPRD UP 70 MPa, 78 l Type IV

Figure 2: Helium concentration close to the ceiling of the tunnel

Test 02 was conducted with a Type IV tank initially filled with 64.5 MPa of helium. Due to an unexpected closure of the solenoid valve at low temperature, the tank was partially emptied. Only 2.5 kg of helium were released out of the 6.5 kg initially in the tank, 2 kg of which were released in about 30 seconds. Over this short period, the helium concentration measured at -6 m at the ceiling reached 5 vol% (Figure 2 b). Moreover, it remained close to 4 vol% for about a hundred seconds. The same behavior was not observed at +6 m. This can be explained by the fact that the discharge being perpendicular to the road, it is slightly inclined with respect to the vertical due to the slope of the tunnel and thus feeds preferentially the negative side of the Y axis. Moreover, the ventilation measured during this test showed a flow from Autrans to Montaud (~0.3 m/s) which reinforces the feeding towards the negative Y axis. Further into the tunnel, the maximum concentrations measured at the ceiling were of the order of 2 vol% (the accuracy of the sensor is close to ±0.1 vol%). Sensors located at +/- 12 and 24 m reacted at about the same time, which confirms the importance of the inertia of the injection. On the other hand, at +/- 50 m the sensor located towards Montaud saw helium before the one located towards Autrans, which seems to be indicative of the effect of the ventilation in the tunnel. Finally, together with the end of the injection and the recovery of the ventilation in the tunnel, the concentration at -6 m increased from 1.5 to 3 vol%. The injection column and the helium rich gas in the area around the point of impact on the ceiling are probably responsible for this increase. The dilution by the external flow of the global ventilation then slowly decreased the helium concentration in the tunnel. A larger extension and a larger quantity associated with a smaller ventilation means that the concentration in the tunnel takes longer to disappear until about 1000 seconds in the lower section of the tunnel (Montaud side), whereas for test 01 in 300 seconds everything had disappeared.

If at the time of the accident the FCHV did not overturn, the release through the TPRD is oriented downward. In the reference situation, a release through a 2 mm hole oriented at 45° towards the rear of the vehicle (test 05) is still considered. In this test 05, of the 6.5 kilograms of helium initially contained in the tank, four kilograms were released in the first forty seconds and an additional kilogram was then released in the following three minutes. This last kilogram was emitted in the form of puffs due to the unexpected closing of the solenoid valve. Although the discharge took place downwards, a concentration higher than 4 vol% was measured on the sensor located in the upper part of the tunnel at -6 m from the injection (Figure 3 a). The other sensors located in the upper part of the tunnel had concentrations equal to 3 vol% at the most. Before injection, a ventilation flow of 0.3-0.4 m/s from Autrans to Montaud was

measured. This can explain the rise in concentration on the sensor located at -24 m (~300 seconds) as well as the very late arrival of helium on the sensor located at -50 m.

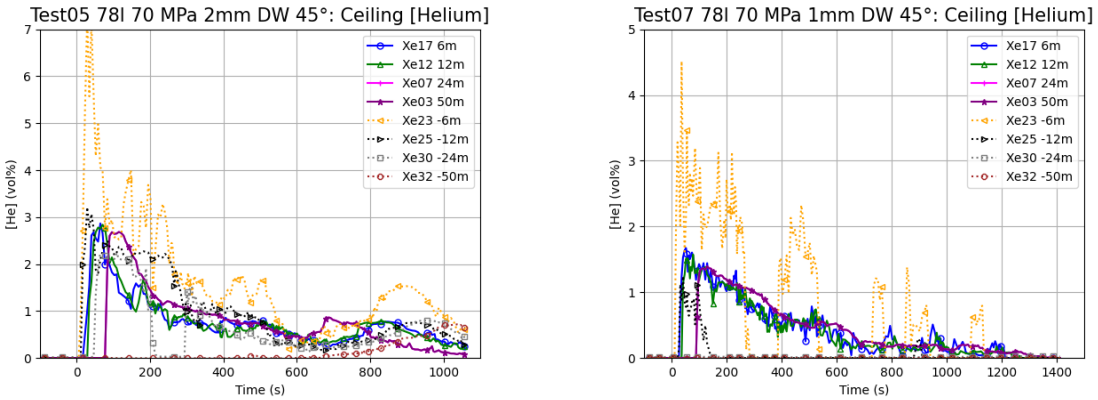

a) Test 05: 2mm TPRD DW 45° 70 MPa, 78 l Type IV

b) Test 07: 1mm TPRD DW 45° 70 MPa, 78 l Type IV

Figure 3: Helium concentration close to the ceiling of the tunnel for a downward 45° release

It is also interesting to examine the helium concentration measured near the chassis (Figure 4). First, under the chassis there was no helium accumulation. Then, above, the concentration was close to the concentration measured at different points of the tunnel cross-section at 0 m, i.e. 1 to 2 vol%. Higher concentrations were measured on the sides and at the back of the chassis, i.e. in the area covered by the impinging discharge. The jet was located very close to the ground (sensor Xe26 closer to the injection showed lower concentration than Xe28 or Xe33) and extended up to 4.5 m behind the chassis. Then, the buoyancy transported the helium to the upper part of the tunnel located at -6 m. A schematic representation of the vertical section of this cloud is provided in green on the Figure 4.

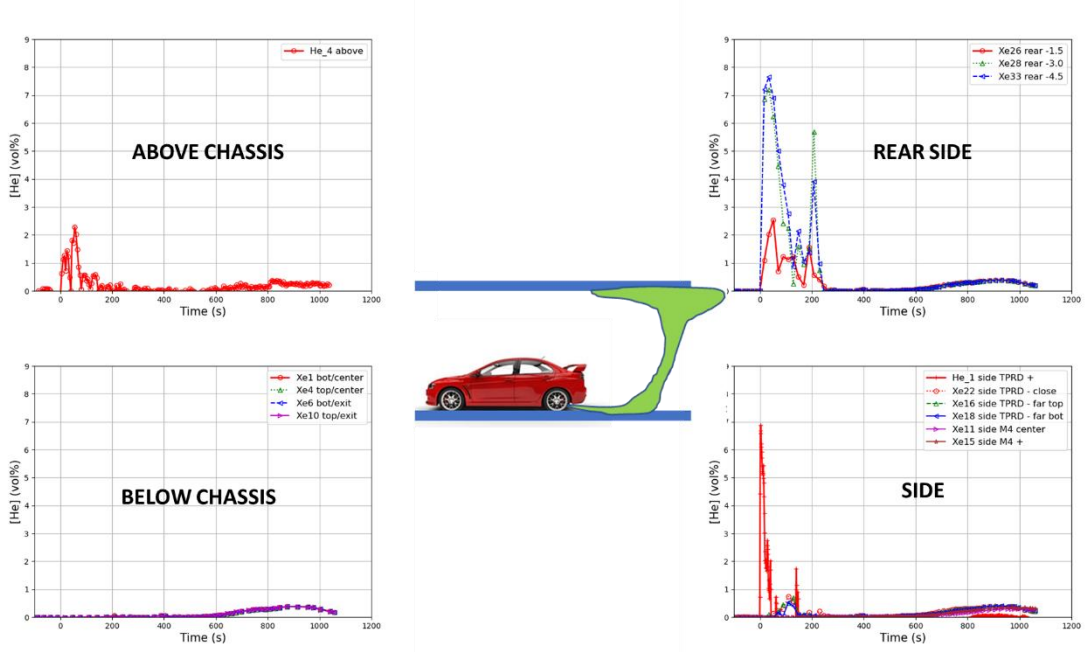

Figure 4: Test 05: Helium concentration close to the chassis.

For comparison, in the 2020 tests, discharges under the chassis but oriented perpendicular to the road were performed. In these tests, the pressure in the tank was only 20 MPa. The helium concentration measurements under the chassis were completely different with very high values up to 20 vol%. Orienting the jet at 45° towards the rear allows to avoid the formation of an explosive atmosphere under

the chassis and to localize it at the rear of the vehicle but up to the top of the tunnel at 6 m behind the car (~5m height).

Decreasing the size of the release orifice to 1mm (Test 07 Figure 3 b) prevents a concentration higher than 4 vol% in the upper part of the tunnel at -6 m. Consequently, the explosive atmosphere no longer reaches the upper part of the tunnel at the beginning of the release. However, it still extends to at least 4.5 m at the rear of the chassis and persists for a longer period due to the longer release time.

In the following, tests 02 and 05 were chosen for the numerical CFD simulations and comparison with experimental results.

3.0 Numerical Models

For this computational exercise, two CFD scale numerical simulation tools were used: the TRUST code with a LES approach to the flow and the Neptune-CFD code with a RANS approach [9]. The first one is developed by CEA while the second one is jointly developed by EDF and CEA.

3.1 Numerical solvers

TRUST solves the Large Eddy Simulation (LES) system of the Navier-Stokes equations for a mixture of two gaseous species, e.g. helium and air of perfect gas. Constant temperature is also assumed. A Wall-Adapted Local Eddy (WALE) viscosity [8] is used to perform the simulations with the coefficient suggested by [10]. As the mesh is very coarse near the walls, a standard wall law is implemented.

The time scheme is a second-order explicit Runge-Kutta scheme. The time step is selected according to Courant-Friedrich-Lewy (CFL) condition of one. A second ordered centred scheme is used to discretize all spatial-derivative terms apart from the convective term where a Quadratic Upstream Interpolation for Convective Kinematics (QUICK) scheme of third order is used.

The Neptune-CFD code is based on a multi-fluid (Eulerian) approach and several validation test cases are related to the gas mixing issues in nuclear containments including hydrogen transport issues. In the present simulations, only the gaseous phase is considered and all the transfer terms between phases are neglected. Two additional transport equations are solved to deal with helium and air in which, the diffusion terms only consider the Fick law with molecular and turbulent diffusion coefficients. Turbulence in the gaseous phase is modelled by the use of a standard two-equation k-epsilon model in which buoyancy production terms are added in both equations and standard wall-functions are used. The buoyancy production term is modeled by:

$$G = -\frac{1}{\rho}\frac{\mu_t}{Pr_t}\overrightarrow{\nabla\rho}.\vec{g} \qquad (1)$$

Where ρ is the density, μ_t the eddy viscosity, Pr_t the turbulent Prandtl number and g the gravity vector. In the turbulent dissipation equation, this term is multiplied by $(1-C_{\varepsilon,3})$ where the constant $C_{\varepsilon,3}=1$ if $G<0$ (stable stratified flow) and 0 instead (unstable stratified flow).

The space discretization is based on a finite-volume approach and the numerical method is based on a fractional steps method called α-P-H cycles to ensure conservation. For the simulation, a variable time-step is used with a maximum CFL number of 1.

3.2 Mesh and boundary conditions

In TRUST, the idealized mesh is composed of 4.8 M hexahedra of various sizes. The size of the cells varies linearly depending on directions that are showed on Figure 5 a. This cross section is extruded in both normal directions to the cross section. The size of the cells is constant to about 10 cm between $y = \pm 2.25$ m, and then the cells size expands linearly from 10 to 50 cm at $y = \pm 75$ m. The total tunnel has

a length of 150 m. The chassis has the exact same location as in the experiment. The injection is represented by a 20 cm sided-square. Sidewalks are also modelled.

The mesh in the section of the release nozzle is given in Figure 5 b for the NEPTUNE-CFD code. Then, this 2D mesh is translated along the tunnel axis to generate the 3D mesh. The local size is gradually increased from the reference size of about 7 cm to 280 cm at +/- 75m. About 1 million of cells is used to mesh the whole tunnel.

A 3D scan of the tunnel was performed in order to simulate the tests with a more representative geometry than the idealized geometries described above. The irregular structure of the tunnel surface can probably affect the local concentrations measured by the sensors. An image of this scan is provided in Figure 5-c along with an illustration of the mesh used in the TRUST calculations presented at the end of the article (Figure 5-d).

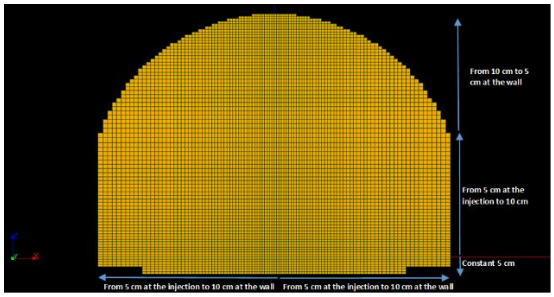

a) TRUST cross-section

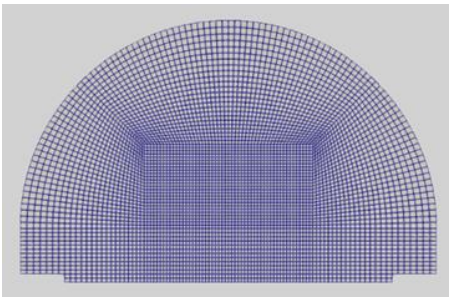

b) NEPTUNE-CFD cross-section

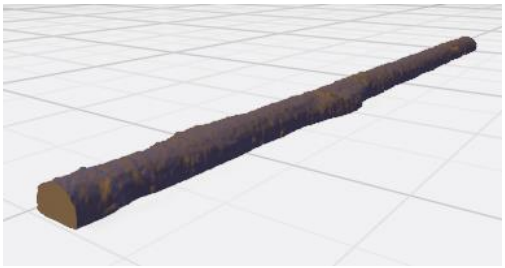

c) 3D scan of the tunnel

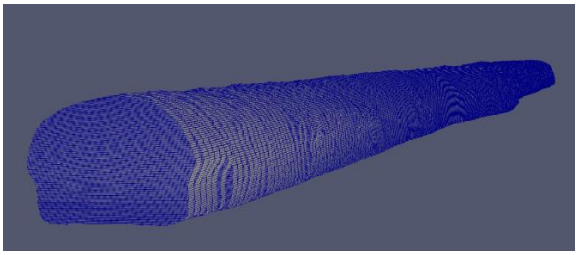

d) 3D mesh of the real tunnel used in TRUST (details close to TPRD)

Figure 5: Meshes used for the CFD computations

Both CFD tools are low Mach number flow solver. Consequently, the highly compressible zone close to an under-expanded jet cannot be adequately modelled. However, these zones have a small volume compared to the tunnel scale and the present study is not focusing on the local flow structures close to an under-expanded jet. For these reasons, our objective is mainly to accurately model the jets after a certain distance where the flow is subsonic. A wide range of hydrogen jets has been studied in the open literature. They can be characterized by dimensionless numbers such as the Froude number and the Mach number defined below:

$$Fr = \frac{U}{\sqrt{\frac{(\rho_a - \rho_{inj})}{\rho_a} gD}} \tag{2}$$

$$Ma = \frac{U}{a} \tag{3}$$

where U is the velocity of the jet at the injection, ρ_{inj} is the density at the injection, ρ_a is the ambient density, g is the acceleration due to gravity, D is the characteristic length of the injection, a is the speed of sound in hydrogen.

The Froude number quantifies the forces that dominates the jet. For $Fr < 10$, the jet is dominated by gravity forces, and for $Fr > 1000$, the jet is dominated by its momentum at the injection. When $10 < Fr < 1000$, the jet is influenced by both gravity and momentum effects. In the test 02 and test 05, the Froude number is around 8000, so the jet is dominated by its initial momentum. Moreover, the jet is sonic at the injection ($Ma > 1$). Several experiments has been conducted to characterize high Froude number supersonic jets. The concentration decay of hydrogen along the jet axis is modelled by the following equation [11], [12]:

$$C_{H_2} = K \sqrt{\frac{\rho_{inj}}{\rho_a}} \frac{D}{x + x_0} \tag{4}$$

where C_{H_2} is the mass concentration of hydrogen on the axis of the jet, x is the distance along the jet axis, x_0 is the virtual origin and K is an empirical constant.

A discharge from a 82 MPa hydrogen tank through a 0,2 mm pinhole [12] is the experiment that is the closest to our case in the tunnel. The coefficient K found is 3,45 and the virtual origin is $x_0 = 45D$, with D the diameter of the injection. Consequently, both CFD models are tuned to predict the same concentration decay at the same distance with the selected meshes. In Neptune-CFD this tuning is made according to the size of the volumetric injection and in TRUST, size of the meshed injection and velocity are adapted to inject the experimental mass flowrate.

Finally, the injected mass flowrate corresponds to the experimental one, including the "puffy" behaviour (Figure 6).

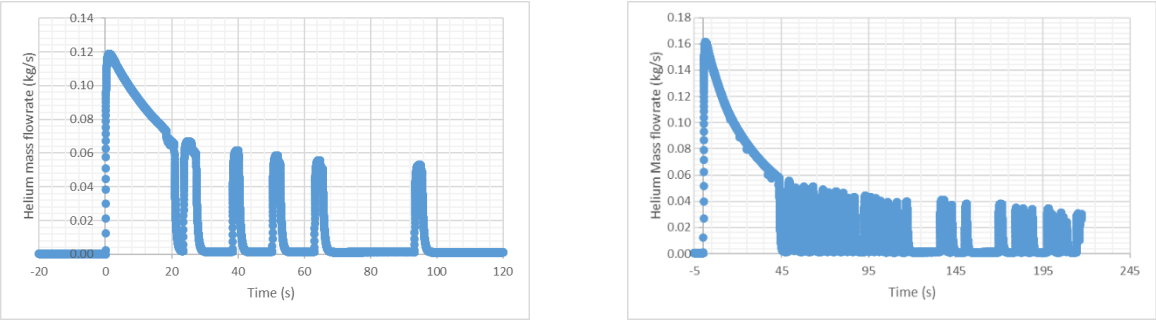

Figure 6: Injected Helium mass flowrates – left: test 02, right: test 05

In the reference computations, the measured external flow due to ventilation of the tunnel is used as boundary conditions on the upper entrance. Prior to the helium release, a computation is performed to develop the initial flow and the boundary layers inside the tunnel.

4.0 Results and discussions

The tunnel-scale helium dispersion calculated for both tests is shown in Figure 7 and Figure 8 for two instants (21 and 100 seconds). The first instant corresponds to the continuous phase of the release while the second one occurs during the puff release phase because during the tests, the main solenoid valve was affected by the temperature drop and closed temporarily. In the first instant (a-pictures), the explosive cloud concentrates in the jet and at the ceiling of the tunnel near the point of impact during a vertical upward injection (Figure 7- a). During downward injection (Figure 8- a), the explosive cloud is concentrated at the rear of the vehicle over a distance of about ten meters. Then, the buoyant nature of the helium becomes visible and the cloud spreads throughout the tunnel section. However, the dilution is sufficient to make the concentration decrease below the 4 vol% chosen as characteristic of the lower flammability limit of hydrogen. At this first moment, the effect of the external flow due to the natural ventilation of the tunnel is not very important. LES and RANS simulations are clearly comparable.

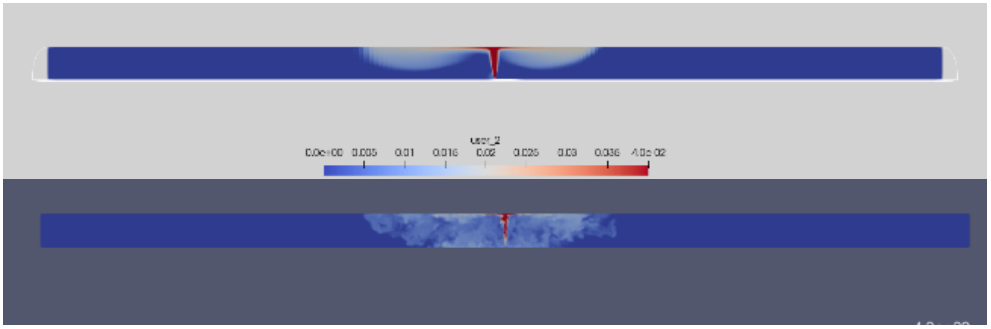

a) t=21 seconds

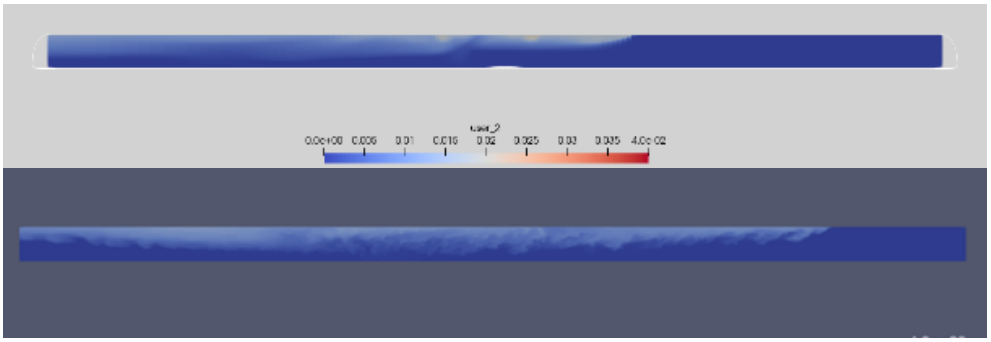

b) t=100 seconds

Figure 7: Test 02 Helium volume concentration (0-4 vol%) on the symmetry plane: left: Neptune-CFD, right: TRUST.

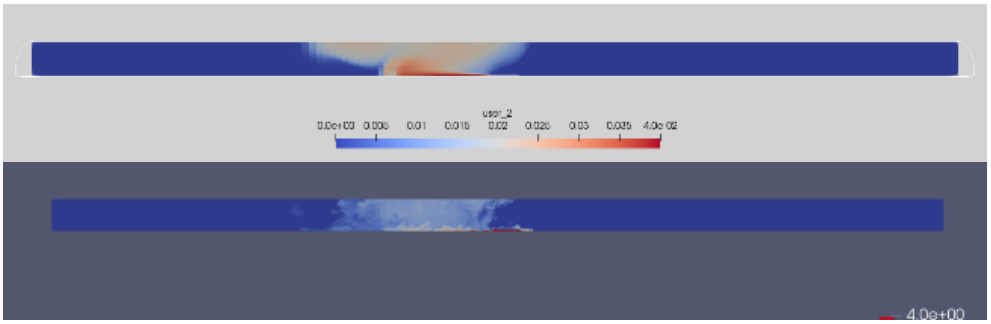

a) t=21 seconds

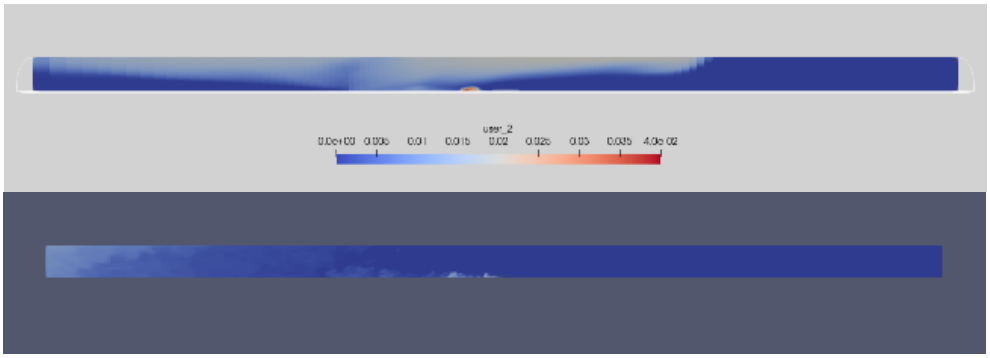

b) t=100 seconds

Figure 8: Test 05 Helium volume concentration (0-4 vol%) on the symmetry plane: top: Neptune-CFD, bottom: TRUST.

On the contrary, at the second instant (b-pictures), the helium is dispersed at the scale of the tunnel and the effect of the external flow can clearly be seen, which tends to convect the cloud towards the lower

part more rapidly than towards the upper part. The dilution is important and the concentration in the cloud is well below 4 vol% eliminating any risk of explosion. LES simulation with a finer mesh tend to predict a larger upward motion for test 02 and downward motion for test 05.

More quantitatively, the comparison between experimental measurements and numerical simulations is provided in Figure 9 for Test 02 and Test 05 focusing on the tunnel-wide measurements and not on the area near the discharge. First, the arrival times of helium in the area between -12 and +12m are relatively well captured by the models for both tests. However, further out, significant differences appear. In test 02, the ascent of the cloud towards the upper entrance is much slower in the RANS model than in the experiment. The cloud does not reach +50m during the 500 seconds simulated whereas experimentally it reaches this position around 200 seconds. LES model behaves better on this particular point probably because of finer mesh. For test 05, the RANS model with only a slight delay much better captures this cloud rise. For the transport to the bottom part, the RANS model also behaves reasonably for the distance of -24m. The differences appear at -50 m: in test 02 the transport is slightly too fast and in test 05, the latter is overestimated by the RANS model because experimentally, the cloud reaches this position much later. LES model behaves differently. The helium transport towards the upper entrance is strongly slowed down in test05 and the overall dilution of helium at the scale of the tunnel is clearly overestimated. For the both simulated concentration levels, the results are always below the measurements, which is indicative of a more important vertical dilution in the models than in the experiment. A finer mesh close to the ceiling of the tunnel can probably improve this point.

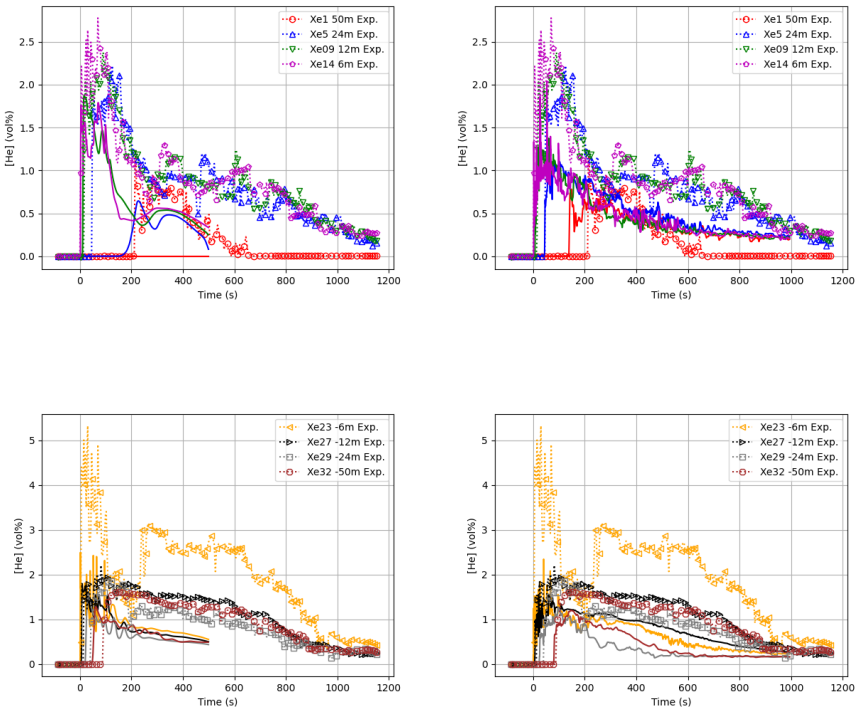

Test 02

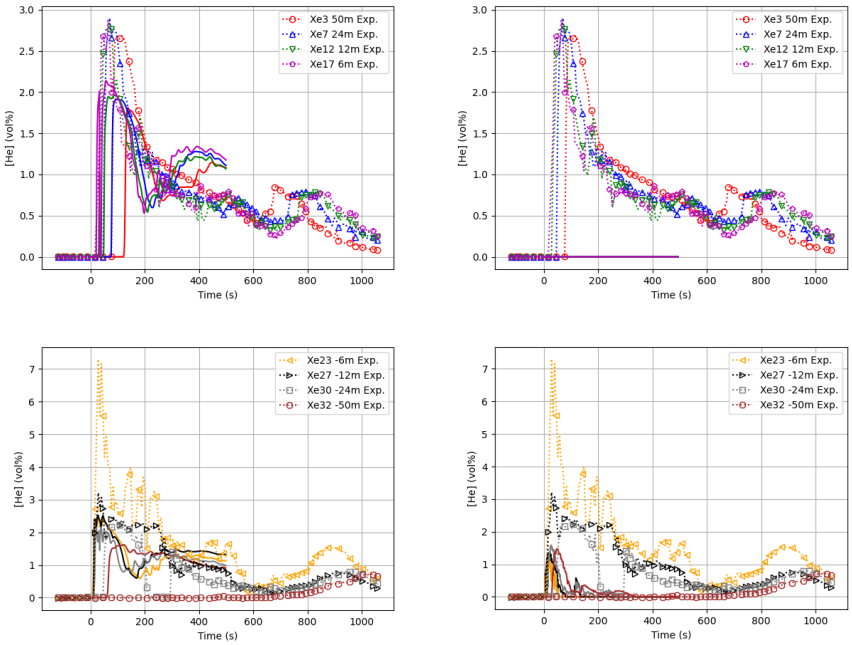

Test 05

Figure 9 : Comparison between experimental measurements (symbol with dotted lines) and numerical simulation (line) for the helium concentration along the ceiling of the tunnel in the central plane and in both axial Y directions – left Neptune-CFD, right TRUST.

The anemometers used to measure the flow in the tunnel were placed about 20 m on either side of the injection point and at a height of about 1.5 m. It is difficult to be sure that these measurements are not affected by the injection. In order to quantify this effect, the calculations of Test 02 were repeated by imposing a constant ventilation flow in the tunnel, corresponding to the flow before the start of the injection. The results (Figure 10) show a better correspondence with the experimental measurements for the arrival times of the cloud on both sides, especially towards the highest part of the tunnel (50 m) for the RANS model. For the LES model, the influence of this boundary condition is clearly less important as well as the calculation in a real geometry.

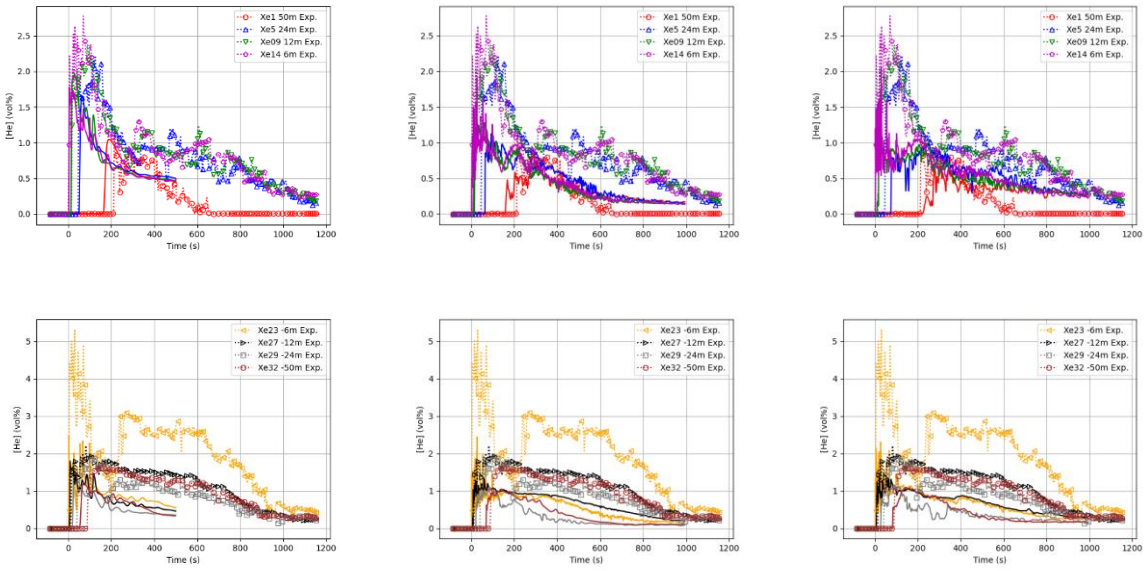

Figure 10 : Test 02 - Comparison between experimental measurements (symbol with dotted lines) and numerical simulation (line) for the helium concentration along the ceiling with a constant ventilation flow – left Neptune-CFD, center TRUST, right TRUST with a mesh corresponding to the scanned tunnel.

5.0 Conclusions and perspectives

From the experimental point of view, in the case of a downward release, tilting the TPRD 45° backwards will prevent the formation of an explosive atmosphere under the vehicle chassis. At the scale of "le tunnel du Mortier" (5.5 m height), a discharge diameter of 2 mm at the bottom up or down leads to the formation of an explosive atmosphere that extends from the bottom to the top of the tunnel but does not extend along the vault. Using a 1 mm diameter greatly restricts this extension but results in a greater persistence of this explosive atmosphere. External convection flow due to natural ventilation (< 1 m/s) does not affect the maximum concentration but drives the transport and dilution of the cloud after the release is complete. The presence of geometric changes in the shape of the tunnel at the top or a highly variable roughness (rock tunnel) can modify the dispersion by preferentially orienting the release, creating areas of accumulation that are more slowly diluted.
From the numerical point of view, two CFD models based on RANS and LES approaches have been set-up to compute two different tests (02 and 05). For the upward release, both models are almost equivalent and comparison with the experimental results and relatively good. The LES model seems less sensitive to boundary conditions such as tunnel ventilation (low air change per hour in our experiments). If the same grid is used for a downward release to the rear at 45°, the differences between the predictions of the two models are larger. In particular, the LES model barely predict a rise in helium to the top of the tunnel. However, the RANS model is much less sensitive to this change and the quality of the results is relatively identical to the upward release case. It therefore seems that for the LES model, an accurate description of the flow near the source (with a dedicated mesh) is an important condition for predictions of helium transport at a more macroscopic scale. Grid sensitivity studies may also improve the results with a finer grid close to the ceiling and they will be part of future sensitivity analyzes.

6.0 Acknowledgements

HyTunnel-CS project has received funding from the FCH2 JU under grant agreements No.826193. This Joint Undertaking receives support from the European Union's Horizon 2020 research and innovation programme, Hydrogen Europe and Hydrogen Europe Research.

References

[1] W. G. Houf, G. H. Evans, E. Merilo, M. Groethe, and S. C. James, "Releases from hydrogen fuel-cell vehicles in tunnels," *11th China Hydrog. Energy Conf.*, vol. 37, no. 1, pp. 715–719, Jan. 2012, doi: 10.1016/j.ijhydene.2011.09.110.
[2] Y. Sato *et al.*, "Hydrogen Release Deflagrations in a Sub-Scale Vehicle Tunnel," presented at the World Hydrogen Energy Conference WHEC 16, Lyon, France, 2006.
[3] D. J. Hall and S. Walker, "Scaling rules for reduced-scale field releases of hydrogen fluoride," *J. Hazard. Mater.*, vol. 54, no. 1, pp. 89–111, Jun. 1997, doi: 10.1016/S0304-3894(96)01856-0.
[4] A. G. Venetsanos, D. Baraldi, P. Adams, P. S. Heggem, and H. Wilkening, "CFD modelling of hydrogen release, dispersion and combustion for automotive scenarios," *Hydrog. Saf.*, vol. 21, no. 2, pp. 162–184, Mar. 2008, doi: 10.1016/j.jlp.2007.06.016.
[5] P. Middha and O. R. Hansen, "CFD simulation study to investigate the risk from hydrogen vehicles in tunnels," *2nd Int. Conf. Hydrog. Saf.*, vol. 34, no. 14, pp. 5875–5886, Jul. 2009, doi: 10.1016/j.ijhydene.2009.02.004.
[6] H. Y. Bie and Z. R. Hao, "Simulation analysis on the risk of hydrogen releases and combustion in subsea tunnels," *Spec. Issue 6th Int. Conf. Hydrog. Saf. ICHS 2015 19-21 Oct. 2015 Yokohama Jpn.*, vol. 42, no. 11, pp. 7617–7624, Mar. 2017, doi: 10.1016/j.ijhydene.2016.05.263.
[7] Y. Li *et al.*, "Numerical analysis of hydrogen release, dispersion and combustion in a tunnel with fuel cell vehicles using all-speed CFD code GASFLOW-MPI," *Int. J. Hydrog. Energy*, Oct. 2020, doi: 10.1016/j.ijhydene.2020.09.063.

[8] D. Bouix *et al.*, “Full-scale tunnel experiments for fuel cell hydrogen vehicles: gas dispersion,” presented at the ICHS 2021, Edinburg, Scotland, 2021.
[9] A. Guelfi *et al.*, “NEPTUNE: A new software platform for advanced nuclear thermal hydraulics,” *Nucl. Eng. Des.*, vol. 156, pp. 281–324, Jul. 2007, doi: 10.13182/NSE05-98.
[10] F. Nicoud and F. Ducros, “Subgrid-scale stress modelling based on the square of the velocity gradient tensor,” *Flow Turbul. Combust.*, vol. 62, no. 3, pp. 183–200, 1999.
[11] J. Xiao, J. R. Travis, and W. Breitung, “Hydrogen release from a high pressure gaseous hydrogen reservoir in case of a small leak,” *Int. J. Hydrog. Energy*, vol. 36, no. 3, pp. 2545–2554, 2011.
[12] K. Okabayashi *et al.*, “Non-steady characteristics of dispersion and ignitability for high-pressurized hydrogen jet discharged from a pinhole,” *Int. J. Hydrog. Energy*, vol. 44, no. 17, pp. 9071–9079, 2019.